MAGNETOHYDRODYNAMICS Vol. 61 (2025), No. 1–2, pp. 55–66
DOI: 10.22364/mhd.61.1–2.6

SEAWATER MAGNETOHYDRODYNAMIC PUMPS AND THRUSTERS: EXPERIMENT, MODEL AND UPSCALING

*Y. Delannoy**, *I. Montero, A. Zapata, N. Machicoane*

Univ. Grenoble Alpes, CNRS, Grenoble INP, LEGI, 38000 Grenoble, France
* *e-Mail: yves.delannoy@grenoble-inp.fr*

Naval magnetohydrodynamic (MHD) propulsion is faced with the high level of Joule dissipation associated with the low electrical conductivity of seawater, reducing the efficiency of the pump at the heart of an MHD thruster. An MHD pump experiment is discussed in this paper, together with its CFD modelling. A simple analytical model is also written for conduction MHD pumps, then for a boat equipped with such a pump working as an MHD thruster. The numerical and analytical results are compared to our pump experiment and to a small-scale boat model. By upscaling, we show how strong should be the magnetic field, and how large the MHD channel to obtain a given efficiency for the pump or a given cruise speed for the boat.

Introduction.

Electromagnetic pumps using steady magnetic fields and conduction through the fluid require low maintenance, are leak-tight due to their rotor-less feature and operate silently. They were developed some decades ago as Magneto-Hydro-Dynamic (MHD) thrusters for naval applications, culminating with the 30-m Yamato boat that reached a speed of 5.5 knots with 4 T superconducting magnets [1]. Recent high-temperature superconducting ribbons [2] may broaden the possibilities if they are integrated onboard in large magnets providing strong magnetic fields in straight channels. This study aims at precising how strong the magnetic field should be to have an efficient pump, and how large the channels should be to have an efficient thruster. We use a simple hydraulic model and a fixed drag coefficient to represent the boat without the channel. To assess this approach, an experimental pump was built inside a superconducting magnet, tested experimentally and described by a CFD model augmented by an MHD module developed in our institution [3]. Furthermore, a model boat was built using permanent magnets in place of superconducting ones, and tested in a pool of artificial seawater.

This paper presents the pump theory and experiment, a simple analytical model for MHD boats and its application to our boat experiments. Using this model for upscaling, some quantitative elements are provided to estimate the necessary magnetic field and the size of such pumps and thrusters.

1. Analytical model of the pump.

A conduction MHD pump is considered here as a straight channel guiding a fluid flow at a velocity $\mathbf{U}$, inserted in a magnet providing a cross flow magnetic field $\mathbf{B}$ and equipped with electrodes forcing a current density $\mathbf{j}$ in the direction of $-\mathbf{U}\times\mathbf{B}$. We assume that those vector fields are perfectly perpendicular and uniform in a brick-shaped domain (Fig. 1) of dimensions L_U, L_B and L_j along each vector field.

The Ohm's law gives $j=\sigma(\Delta\varphi/L_j - UB)$, where $\sigma \approx 5\,\Omega^{-1}\mathrm{m}^{-1}$ is the conductivity of seawater and $\Delta\varphi$ is the potential difference imposed to the solution by the electrodes. Because of electrolysis in the ionic solution, the anode (resp. cathode) is at a potential $E_\mathrm{a}>0$ (resp. $E_\mathrm{c}<0$) with respect to the solution nearby, and the voltage difference between the electrodes, $\Delta\varphi_\mathrm{el}=\Delta\varphi+(E_\mathrm{a}-E_\mathrm{c})$ contains an electrochemical term

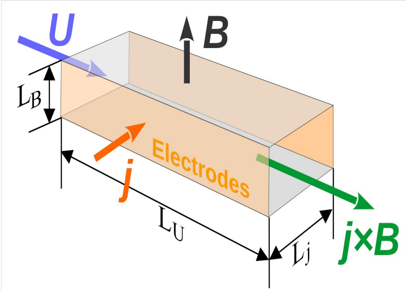

Fig. 1. Schematic presentation of the MHD channel.

$E_a - E_c \sim 2\,\mathrm{V} \to 6\,\mathrm{V}$ for $j \sim 0 \to 1\,\mathrm{kA/m^2}$ [4]. Multiplying by the total current $I = jL_U L_B$ we obtain the total electrical power P_{el}, its part P_{chim} consumed by electrochemical reactions and the rest P_{channel} transferred to the solution:

$$P_{\mathrm{el}} = I\Delta\varphi_{\mathrm{el}}, \quad P_{\mathrm{chim}} = I(E_a - E_c), \quad P_{\mathrm{channel}} = I\Delta\varphi. \tag{1}$$

Note that the ratio $\eta_{\mathrm{chim}} = P_{\mathrm{channel}}/P_{\mathrm{el}}$ is usually greater than 0.9 or higher for large size channels.

From the Ohm's law, we find that $\Delta\varphi = RI + UBL_j$, where $R = L_j/(\sigma L_U L_B)$ is the electrical resistance of the channel and UBL_j is the counter-electromotive force due to the fluid velocity. Multiplying by I, we find the Joule dissipation RI^2, i.e. the integral of j^2/σ and the integral of $f_L U$ (where $f_L = j_B$ is the Lorentz force), i.e. the mechanical power transferred to the fluid:

$$\Delta\varphi = RI + UBL_j \Rightarrow P_{\mathrm{channel}} = P_{\mathrm{joule}} + P_{\mathrm{mhd}}; \quad P_{\mathrm{joule}} = RI^2; \quad P_{\mathrm{mhd}} = IBUL_j. \tag{2}$$

Of course, P_{joule} is lost for propulsion or pumping, and maximizing the MHD efficiency $\eta_{\mathrm{mhd}} = P_{\mathrm{mhd}}/P_{\mathrm{channel}}$ is a key point of any design. As for any electric receiver, $\eta_{\mathrm{mhd}} = UB/(\Delta\varphi/L_j)$ increases when the applied voltage $\Delta\varphi$ decreases towards the counter-electromotive force UBL_j, but then the current vanishes and the thrust or pump head vanishes also.

As in any hydraulic pump, the mechanical power P_{mhd} is partly dissipated by the friction inside the pump, and the external circuit may only use the remaining part, i.e. the hydraulic power $P_{\mathrm{hyd}} = Q\Delta p_{\mathrm{tp}}$ convected out of the pump by the flowrate $Q = UL_B Lj$ flowing in the pump. Here Δp_{tp} is the total pressure (or head) supplied by the pump (mechanical energy per unit volume of fluid). This head Δp_{tp} corresponds to a pressure rise in a straight channel as the one in Fig. 1, but it may also include a variation of the kinetic energy per unit volume, $\rho U^2/2$, if the section evolves along the channel. The head loss Δp_{loss} is expressed using a head loss coefficient k_{loss} (considered constant here), and P_{mhd} is expressed from Eq. (2), so that

$$P_{\mathrm{mhd}} = P_{\mathrm{loss}} + P_{\mathrm{hyd}}; P_{\mathrm{hyd}} = Q\Delta p_{\mathrm{tp}} \Rightarrow \Delta p_{\mathrm{tp}} = (B/L_B)I - (k_{\mathrm{loss}}/2)\rho U^2. \tag{3}$$

Note that k_{loss} is an important parameter containing regular losses fL_U/D_{hyd}, where $D_{\mathrm{hyd}} = 4L_B L_J/(2L_B + 2L_J)$ is the hydraulic diameter and f is the friction factor, but also minor losses due to entry effects or to geometric imperfections. The friction factor depends on the wall rugosity divided by D_{hyd}, and possibly on the velocity except at very high Reynolds numbers. The hydraulic efficiency $\eta_{\mathrm{hyd}} = P_{\mathrm{hyd}}/P_{\mathrm{mhd}}$ is, therefore, difficult to predict.

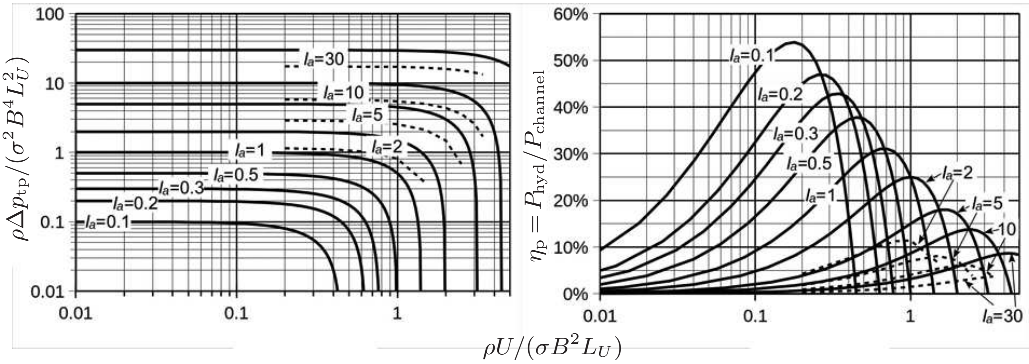

Fig. 2. Dimensionless characteristics for $k_{\mathrm{loss}} = 1$. Dashed lines for the pump experiment (part 2).

Eq. (3) represents the characteristic of the pump for a given current I. A dimensionless equivalent can be built using reference values based on B, σ, ρ, L_U, i.e. on the fixed design parameters. The dimensionless velocity $U_{\mathrm{a}} = \rho U/(\sigma B^2 L_U)$ is the inverse of the Stuart number and is also a dimensionless flowrate: $U_{\mathrm{a}} = \rho Q/(\sigma B^2 L_U L_B L_J)$. The dimensionless current density (and dimensionless current) is

$$I_{\mathrm{a}} = \rho j/(\sigma^2 B^3 L_U) = \rho I/(\sigma^2 B^3 L_U^2 L_B).$$

Eq. (3) becomes

$$\Delta p_{\mathrm{ta}} = I_{\mathrm{a}} - k_{\mathrm{loss}} U_{\mathrm{a}}^2/2, \tag{4}$$

where

$$U_{\mathrm{a}} = \frac{\rho U}{\sigma B^2 L_U}, \quad \Delta p_{\mathrm{ta}} = \frac{\rho \Delta p_{\mathrm{tp}}}{\sigma^2 B^4 L_U^2}, \quad I_{\mathrm{a}} = \frac{\rho I}{\sigma^2 B^3 L_U^2 L_B}.$$

The pump efficiency $\eta_{\mathrm{p}} = \eta_{\mathrm{mhd}}\eta_{\mathrm{hyd}} = P_{\mathrm{hyd}}/P_{\mathrm{channel}}$ may also be expressed using U_{a} and I_{a} as

$$\eta_{\mathrm{p}} = \frac{U_{\mathrm{a}}}{I_{\mathrm{a}}} \cdot \frac{I_{\mathrm{a}} - k_{\mathrm{loss}} U_{\mathrm{a}}^2/2}{I_{\mathrm{a}} + U_{\mathrm{a}}}. \tag{5}$$

Eq. (4) and Eq. (5) are plotted in Fig. 2 for a loss coefficient $k_{\mathrm{loss}} = 1$ representative of the MHD pump and model boat studied experimentally by our team. A lower value of k_{loss} would, for each value of I_{a}, enlarge the range of the flowrate available before the head drops, and increase the maximum efficiency that is reached just before this dropout.

2. Experimental helical channel pump.

An existing superconducting magnet was equipped with a tank in its 45 cm-diameter bore, inside which a helical channel between two cylindrical concentric electrodes constituted an MHD pump, connected to an external hydraulic circuit (Fig. 3). The vertical magnetic field B_{ctr} reached up to 4 T at the center point of the spiral channel and four experimental runs were performed at $B_{\mathrm{ctr}} = 3$, 3.5 and 4 T.

The tank features anti-vortex grids to damp the tangential flow running out of the helical channel. Electrodes made of titanium for its resistance to corrosion are platinum-coated for electrochemical properties. A regulating valve could be installed in the external hydraulic loop to change its hydraulic resistance. For each experimental run, four configurations were tested: without vane (SV), with the vane fully open (VO), with the vane closed at 60% (V11) and with a varying position of the vane ("Vanne Variable"). For this

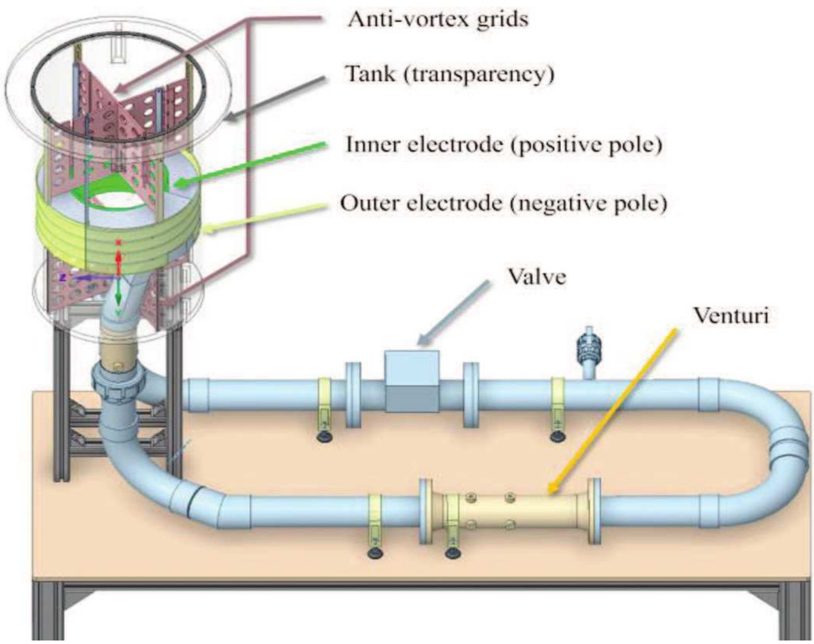

Fig. 3. Geometry of the MHD channel.

last configuration, the power supply was used at a fixed voltage $\Delta\varphi_{\mathrm{el}} = 10\,\mathrm{V}$, whereas for SV, VO and V11, $\Delta\varphi_{\mathrm{el}}$ varied from 4 V to 20 V.

The flowrate Q was measured using a Venturi installed in the external hydraulic loop and connected to a differential pressure sensor. The helical channel is equipped with six pressure taps drilled through the inner electrode, connected by flexible tubes through the bottom of the tank to absolute pressure sensors. Those taps are spaced half a turn apart along the helical channel, with tap number 1 located a quarter turn from the inlet and tap 6 a quarter turn from the outlet. All the pressure sensors are located 3.5 m away from the magnet center to protect them from the magnetic field influence.

The current I supplied to the electrodes was measured by a clamp ammeter, and two potentiostats were used to measure the anode and cathode potentials ($E_{\mathrm{a}} > 0$ and $E_{\mathrm{c}} < 0$) with respect to a reference silver wire just protruding from the electrode into the salt water.

Starting from the Ohm's law, it can be shown that the voltage $\Delta\varphi = \Delta\varphi_{\mathrm{el}} - (E_{\mathrm{a}} - E_{\mathrm{c}})$ applied to the ionic solution should contain a resistive term and a counter-electromotive term due to the displacement of the conductor in the magnetic field (see Section 1 for a detailed development in a straight channel):

$$\Delta\varphi = cQB + RI \Rightarrow \Delta\varphi_{\mathrm{el}} = (E_{\mathrm{a}}^0 - E_{\mathrm{c}}^0) + cQB + (R + R_{\mathrm{ch}})I. \tag{6}$$

Note that the "electrochemical voltage loss" E_{a} - E_{c} has a minimal value $E_{\mathrm{a}}^0 - E_{\mathrm{c}}^0$ at low current related to the thermodynamic potentials of the species involved in the electrolysis reactions, and it grows with the current density because of kinetic effects. Assuming, to the first order, that this increase occurs at a constant slope (i.e. $\mathrm{d}(E_{\mathrm{a}} - E_{\mathrm{c}})/\mathrm{d}I = C^{\mathrm{st}} = R_{\mathrm{ch}}$), we derive the second form in Eq. (6).

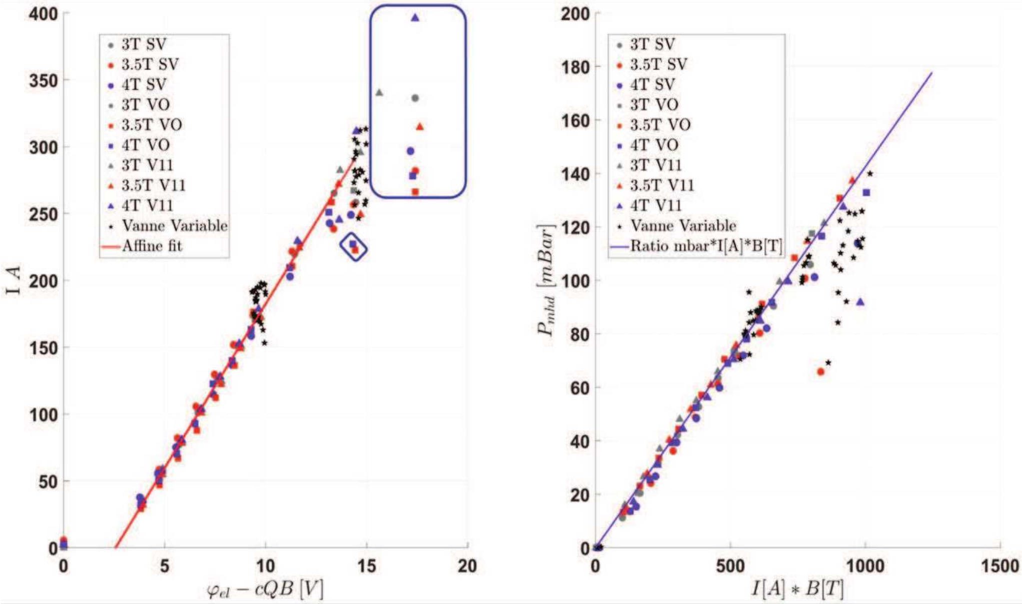

Fig. 4. Current versus voltage (left) and MHD pressure head versus IB (right) for all experiments.

To highlight this behavior in our experiments, we adjusted the constants $(E_\mathrm{a}^0 - E_\mathrm{c}^0)$, $R + R_\mathrm{ch}$ and c of the above equation to best fit (in the least squares sense) the 149 experimental results obtained at $\Delta\varphi_\mathrm{el} \leq 14\,\mathrm{V}$ (Fig. 4). Results at higher voltages are disturbed by the presence of gas in the channel due to electrolysis at the electrodes. Those points are not included in the analysis discussed herein, nevertheless, we plotted them in Fig. 4 (points inside frames) together with the other points used for further analysis.

The best fit is obtained for $E_\mathrm{a}^0 - E_\mathrm{c}^0 = 2.57\,\mathrm{V}$, $R + R_\mathrm{ch} = 0.0407\,\Omega$, $c = 31.6\,\mathrm{m}^{-1}$. Excluding several cases perturbed by bubbles attached to the silver wires, the potentiostat gave several values of $E_\mathrm{a} - E_\mathrm{c}$. Subtracting to $\Delta\varphi_\mathrm{el}$, we have $\Delta\varphi = RI + cUB$ (not shown here) that can be correlated by $R = 0.0227\,\Omega$.

From the pressure measurements at taps # 1 and # 6 (five half-turns apart), we can reconstruct their difference Δp_{61} which is a large part of the pressure head of the pump (the pump has a total of six half-turns). Due to the Lorentz force, this head includes a positive term proportional to the current and to an appropriate average of the magnetic field, itself being proportional to B_ctr. Because of the head loss inside the helical channel, it also includes a negative term proportional to Q^2,

$$\Delta p_{61} = a_{61} I B_\mathrm{ctr} - K_{61} Q^2. \tag{7}$$

We suppose here that the Reynolds number (of order 10^5) is sufficiently high to have a constant hydraulic resistance K_{61} whatever the flowrate [5]. Other studies [6] also used a_{61}, the pressure gain achieved for each unit of IB. Fitting of the MHD experiments provided the following coefficients:

$$a_{61} = 0.1457\,\mathrm{mbar/(A/T)}; \quad K_{61} = 0.0273\,\mathrm{mbar/(m^3/h)^2}.$$

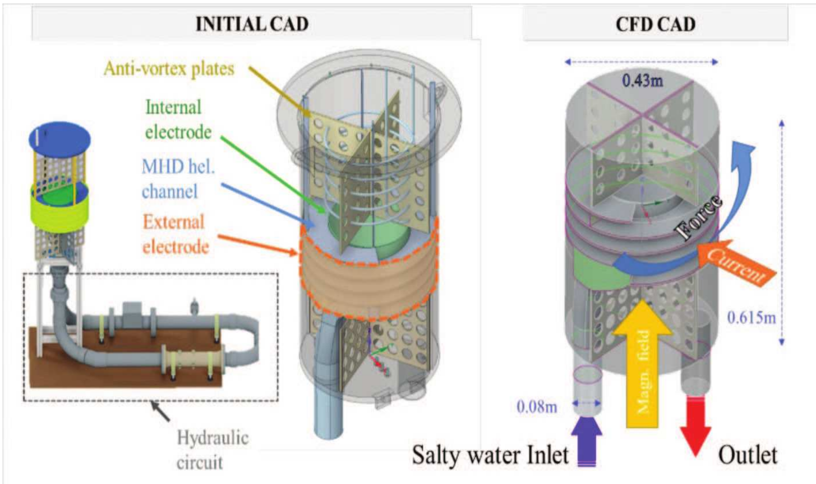

Fig. 5. MHD helicoidal canal (blue) inside the vessel (grey) with vortex-breaking grids (yellow). The inner wall of the channel (green) and the outer wall (orange) are concentric electrodes.

The fit is illustrated in Fig. 4, where we have plotted $\Delta p_{\mathrm{mhd}} = \Delta p_{61} + K_{61}Q^2$ as a function of IB. Note that the head loss $K_{61}Q^2$ is a minor correction ($\leq$17 mbar) to the pressure head, and that it has been validated at $B = 0$ using an auxiliary pump to provide the flowrate.

3. CFD model of the pump.

The numerical model was developed using ANSYS$^{\mathrm{TM}}$, and the MHD steady 3D turbulent flow was solved with Fluent$^{\mathrm{TM}}$ and MHD User Defined Functions (UDF) [3].

In the CFD model (Fig. 5), the hydraulic circuit is replaced by an inlet into the tank, where the flowrate measured in the experiments is imposed, and by a pressure condition at the tank outlet. The electrical potential applied to the electrodes is adapted to reach the current measured in the experimental setup. The top part of the tank is a zero wall shear stress because it models a fixed free surface. The superconductor magnet, located around the vessel and centred on the MHD channel, is modelled separately using our UDF module as a 2D axisymmetric electromagnetic model, then the B-field is interpolated on the 3D mesh. Regarding the pressure in the MHD channel, six pressure values were extracted at the same locations as the pressure sensors in the experimental setup.

The mesh is polyhedral because it usually leads to a better and faster convergence [7]. It is a one million cells mesh including a prism layer of six cells on each wall, with a first layer height of 150 μm, connected with continuity of size to the polyhedral volume mesh. With such a prism layer, the first discretisation point is at a dimensionless distance $y^+ \approx 30$ of the wall in most parts of the MHD channel.

CFD simulations were conducted at three levels of the magnetic field and nine values of the flowrate for each magnetic field (corresponding to the experiments in the SV configuration, see section 2). The calculated values of $\Delta\varphi$ and Δp_{61} are compared to the experiments in Fig. 6. Considering the total Joule power dissipated in the whole domain, we also obtained the resistance of the fluid $R = P_{\mathrm{joule}}/I^2$. Its calculated value $R = 0.0248\,\Omega$ is close to the experimental value $R = 0.0227\,\Omega$.

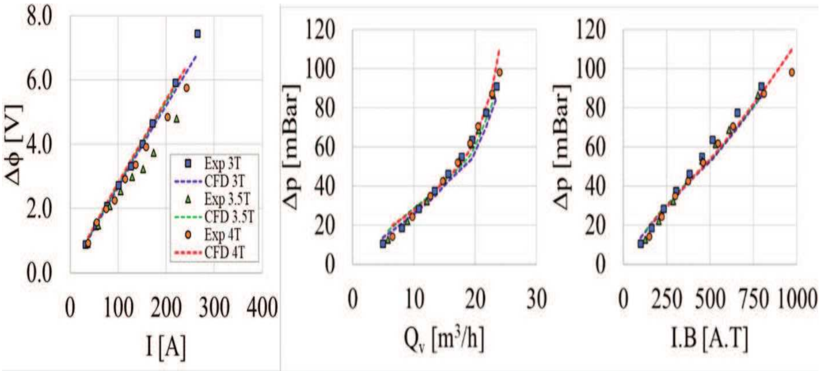

Fig. 6. (Left) Voltage applied to the solution versus the current through the electrodes. (Centre) Pressure difference Δp_{61} between pressure taps 6 and 1 versus the volumetric flowrate. (Right) Evolution of the same pressure difference according to Laplace force term IB_{ctr}.

Table 1. Calculated and experimental characteristics of the electromagnetic pump.

Flowrate Q [m^3/h]	17.75		19.31	
Reynolds number	$8 \times 10^4 \sim 9 \times 10^4$			
Hartmann number	21.5		28.4	
Magnetic field B_{ctr} [T]	3		4	
Powers and losses [W]	**Exp.**	**CFD**	**Exp.**	**CFD**
P_{el}	1362	Not calculated	1231	Not calculated
P_{chim}	756	Not calculated	770	Not calculated
P_{channel}	606	606 (+0.07%)	461	516 (+12%)
P_{joule}	568	566 (–0.39%)	414	464 (+12%)
P_{mhd}	38	41 (+7%)	47	52 (+11%)
P_{loss}	6	12 (+107%)	7	15 (+108%)
P_{hyd}	32	29 (–11%)	40	37 (–6%)

Regarding the pressure rise in the MHD channel, the CFD calculations are in fair agreement with the experimental data; the CFD model can predict accurately the hydraulic behaviour of the electromagnetic pump. Moreover, the pressure rise in the MHD channel is approximately proportional to IB, i.e. to the Laplace–Lorentz force, because the head loss term is small compared to that pressure rise. The calculated powers and losses in the pump are compared in Table 1 to the experiments for $\Delta\varphi_{\mathrm{el}}$– 9 V and two different magnetic fields.

The numerical MHD modelling of the electromagnetic pump with the Fluent$^{\mathrm{TM}}$ CFD solver is promising. It was able to match fairly the experimental data both in terms of electrical and hydrodynamic behaviour. Some flaws are to be mentioned, such as the electrochemistry and the external hydraulic circuit that were obtained only from the experiment.

4. Theory for MHD boats.

An MHD boat (sketched in Fig. 7) is equipped with a propulsion channel comprising an MHD pump (see Fig. 7), an inlet section, often converging, and an outlet section that

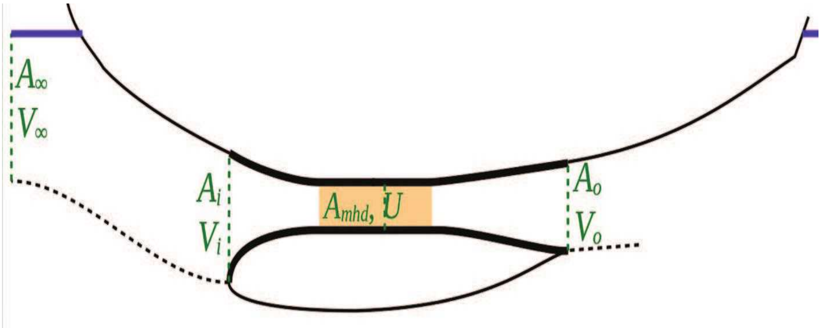

Fig. 7. Propulsion channel of an MHD boat.

may be slightly diverging (with the risk of detachment and high head loss). The figure also shows the flow tube passing through the thruster and its upstream section, where the fluid velocity V_∞ is equal to the boat speed, and the relative modified pressure p^*_∞ is 0. The areas A_i and A_0 of the inlet and outlet sections are known from their ratios $\alpha_\mathrm{i} = A_\mathrm{i}/A_\mathrm{mhd}$ and $\alpha_0 = A_0/A_\mathrm{mhd}$ to the crossflow section $A_\mathrm{mhd} = L_B L_J$ of the MHD channel. We use here $\alpha_0 = 1$ because a divergent nozzle will produce detachments and reduce the boat speed (see experiment in part 5), and $p^*_0 = 0$ since the jet is in equilibrium with the external water flow, which is similar to a wake flow in this region. Then a momentum balance on the propeller (section between A_i and A_0) gives the thrust:

$$T = \left[\rho U^2 \left(1 - 1/\alpha_\mathrm{i}\right) - p^*_\mathrm{i}\alpha_\mathrm{i}\right] A_\mathrm{mhd} \tag{8}$$

The thrust in Eq. (8) includes the reaction to the MHD force applied to water, but also the pressure and friction forces applied on the internal walls of the thruster (bolded lines in the figure), generally downstream (drag) and balancing a large part of the MHD reaction force.

When the boat speed is stable (cruise conditions), the thrust equilibrates the drag of the boat (excluding the inner drag of the channel), expressed here using a constant drag coefficient C_D and the projected frontal area S of the boat. We suppose that the inlet is adapted to the cruise velocity, i.e. $p^*_\mathrm{i} = 0$. This is obtained only for $\alpha_\mathrm{i} = (U/V_\infty)_\mathrm{cruise}$, any other values will decrease the thrust but only weakly. The thrust to drag equilibrium becomes:

$$\rho U^2 A_\mathrm{mhd}\left(1 - \frac{V_\infty}{U}\right) = SC_\mathrm{D}\frac{\rho V_\infty^2}{2} \Rightarrow \left(\frac{U}{V_\infty}\right)^2 - \frac{U}{V_\infty} \Rightarrow \frac{U}{V_\infty} = \frac{1}{2}\left(1 + \sqrt{1 + 2\alpha_\mathrm{SCD}}\,\right) \tag{9}$$

where $\alpha_\mathrm{SCD} = SC_\mathrm{D}/A_\mathrm{mhd}$ is a dimensionless drag section, increasing with the drag coefficient and decreasing when the part of the front section occupied by the thruster increases.

The channel velocity is given as a function of the pump regime (i.e. of IB), by the generalized Bernoulli equation from A_∞ to A_0, including the pump head (Eq. (3)) and additional losses due to the inlet section and the outlet nozzle (k_tot represent the hydraulic loss between A_i and A_0):

$$\frac{\rho U^2}{2} = \frac{\rho V_\infty^2}{2} - k_\mathrm{tot}\frac{\rho U^2}{2} + \frac{IB}{L_B}. \tag{10}$$

Eliminating U between Eq. (9) and Eq. (10) we obtain the boat cruise speed V_∞ as a function of the pump regime. Dividing it by $\sigma B^2 L_U/\rho$ and I by $\sigma^2 B^3 L_U^2 L_B/\rho$ (as in section 1) gives the dimensionless form:

$$\frac{\rho V_\infty^2}{2} = \frac{4IB/L_B}{(1+k_{\text{tot}})\left(1+\sqrt{1+2\alpha_{\text{SCD}}}\right)^2 - 4} \Rightarrow V_{\infty,\alpha}^2 = \frac{2I_{\text{a}}}{(1+k_{\text{tot}})\beta^2 - 1}, \tag{11}$$

where

$$\beta = \frac{1}{2}\left(1+\sqrt{1+2\alpha_{\text{SCD}}}\right)$$

Here, β is a shorthand for the group giving U/V_∞, Eq. (9). Using the Ohm's law in $P_{\text{channel}} = I\Delta\varphi$ and Eq. (8) for the thrust T, we can write them in a dimensionless form using the volume $V_{\text{mhd}} = A_{\text{mhd}}L_U$:

$$T_{\text{a}} = V_{\infty,\alpha}^2(\beta^2 - \beta), \quad P_{\text{ch,a}} = I_{\text{a}}(I_{\text{a}} + \beta V_{\infty,\alpha}^2), \tag{12}$$

where

$$T_{\text{a}} = \frac{\rho T}{\sigma^2 B^4 L_U V_{\text{mhd}}}, \quad P_{\text{ch,a}} = \frac{\rho^2 P_{\text{channel}}}{\sigma^3 B^6 L_U^2 V_{\text{mhd}}}.$$

The thruster efficiency $\eta = TV_\infty/P_{\text{channel}}$ is constructed from the useful power DV_∞ (with $D = T$) as

$$\eta = \frac{\eta_{\max}}{1 + V_{\infty,\text{a}}/V_{\text{a,ref}}} \tag{13}$$

with

$$\eta_{\max} = \frac{2(1-\beta)}{(1+k_{\text{tot}})\beta^2 - 1}$$

and

$$V_{\text{a,ref}} = \frac{2\beta}{(1+k_{\text{tot}})\beta^2 - 1}.$$

In any reaction thruster, the efficiency is limited by $\eta_{\max}$ that takes into account the internal hydraulic loss (k_{tot}) and the kinetic energy lost in the jet (from $\beta = U/V_\infty$). An MHD thruster then divides this efficiency by $1 + V_\infty/V_{\text{ref}}$, where

$$V_{\text{ref}} = \frac{\sigma B^2 L_U/\rho}{2\beta/[(1+k_{\text{tot}})\beta^2 - 1]}$$

represents the boat velocity above which the efficiency is divided by more than twice. Since this reference velocity increases with $B^2 L_U$, we can know how to estimate the size and magnetic field necessary to have a correct efficiency (see section 5).

5. Validation and upscaling.

The main parameters of the pump experiment (sections 2 and 3) and the model boat developed in our laboratory are summarized in Table 2. The salinity of water was 35 g/l for the boat and 200 g/l for the pump (to increase σ). The values of B is the component

Table 2. Parameters of the experiments.

	L_U [mm]	L_B [mm]	L_J [mm]	σ [Ω^{-1}m^{-1}]	ρ [kg/m^3]	B [T]	S [m^2]
Pump exp.	3200	39	80	19.5	1163	3.51; 4.09; 4.68	–
Model boat	100	28	32.5	5.26	1025	0.57	0.0163

along L_B, averaged for the MHD channel. The three values for the pump correspond to $B_{\mathrm{ctr}} = 3\,\mathrm{T}$; $3.5\,\mathrm{T}$; $4\,\mathrm{T}$ at the centre of the magnet. The front section of the boat takes into account the real immersion of the hull.

For the pump (that has a 3-turns helical channel instead of a straight one as in Fig. 1), we measured experimentally the channel voltage $\Delta\varphi$ and the pressure gain $\Delta p_{\mathrm{t},61}$ produced by 2.5 turns of the helix. All experiments (for $30\,\mathrm{A} < \mathrm{I} < 300\,\mathrm{A}$ and $2.5\,\mathrm{m}^3/\mathrm{h} < \mathrm{Q} < 25\,\mathrm{m}^3/\mathrm{h}$) were fit by $\Delta\varphi = R_{\mathrm{exp}} I + cQB_{\mathrm{ctr}}$ with R_{exp}=0.7mΩ, c=31.62m^{-1}, and by $\Delta p_{\mathrm{t},61} = a_{61} I B_{\mathrm{ctr}} - K_{61} Q^2$ with $a_{61} = 14.57\,\mathrm{m}^{-1}$ and $K_{61} = 3.54 \times 10^7\,\mathrm{Pa{\cdot}s^2/m^6}$. To add the sixth half turn, we multiply the first term of $\Delta p_{\mathrm{t},61}$ by 1.195 (from our magnetic field calculation) and the second one by 1.2 (= 6/5). We also take into account that $B_{\mathrm{ctr}} = B/1.17$ and $Q = UL_J L_B$. Our experimental laws than become:

$$\begin{cases} \Delta\varphi & = R_{\mathrm{exp}} I + dUB, \\ \Delta p_{\mathrm{t,pump}} & = aIB - (k_{\mathrm{loss}}/2)\rho U^2 \end{cases} \tag{14}$$

with $R_{\mathrm{exp}} = 40.7\,\mathrm{m}\Omega$, $d = 84.3\,\mathrm{mm}$, $a = 14.88\,\mathrm{m}^{-1}$ and $k_{\mathrm{loss}} = 0.711$.

Note that a and R_{exp} differ from the values L_B^{-1}=25.6m^{-1} and $L_J/(\sigma L_U L_B)$=32.9mΩ that would be obtained for a straight channel (section 1) because of the different distribution of the current density in the helical channel. However, d is close to the value $L_J = 80\,\mathrm{mm}$ obtained in section 1. The loss coefficient also differs from the regular loss coefficient $k_{\mathrm{th}} = 1.3$ calculated for a straight pump channel with the same dimensions at a flowrate of $20\,\mathrm{m}^3/\mathrm{h}$. Switching to dimensionless forms and constructing the pump efficiency yield

$$\begin{aligned} \Delta p_{\mathrm{ta}} &= aL_B I_a - \frac{1}{2} k_{\mathrm{loss}} U_a^2, \\ \eta_{\mathrm{pump}} &= \frac{U_a}{I_a} \frac{aL_B I_a - (k_{\mathrm{loss}}/2U)_a^2}{(R_{\mathrm{exp}}\sigma L_U L_B/L_I) I_a + (d/L_I) U_a} \end{aligned} \tag{15}$$

for $0.19 < U_a < 3.4$ and $2.2 < I_a < 53$.

Those laws are illustrated in Fig. 5 together with the theoretical laws for straight channels, showing a qualitative agreement and also that the efficiency could only be improved with a lower current and a lower velocity (at the expense of a lower head produced by the pump!). The numerical approach (section 3) is closer to experiments, since it uses a spiral channel and the real distributions of **B** and **j**.

In our model boat (Fig. 8) a transparent plate in the rear part initially produced a diverging nozzle ($\alpha_0 = 3$), and was then removed ($\alpha_0 = 1$). The boat speed reached $0.2\,\mathrm{m/s}$ with the rear plate and $0.3\,\mathrm{m/s}$ without it. A CFD study showed strong recirculations in the divergent when equipped with the plate, and a smooth mixing with the outer flow when this plate was removed. Therefore, we adopted a straight outlet ($\alpha_0 = 1$) to describe our model without the plate. The loss coefficient of the channel (without a diverging nozzle) was estimated to $k_{\mathrm{tot}} = 1$ (among which $k_{\mathrm{loss}} = 0.8$ for the MHD channel). With the current $I = 21\,\mathrm{A}$ measured in the experiment, our model, Eq. (11), gives the experimental cruise speed of $0.3\,\mathrm{m/s}$ for $C_{\mathrm{D}} = 0.27$, what seems reasonable for such a hull. Then $\beta = 2.14$, showing that the inlet section is almost adapted to the cruise speed ($\alpha_{\mathrm{i}} = 3$ is not far from $\mathrm{U}/V_\infty = 2.14$), and $\eta_{\max} = 28\%$, what could be increased with a better hydraulic design (decreasing k_{tot} and/or C_{D}), or with a larger channel (decreasing α_{SCD}). However, at $V_\infty = 0.3\,\mathrm{m/s}$, $\eta = 0.0083\%$ is far below $\eta_{\max}$ since $V_{\mathrm{ref}} = 9 \times 10^{-5}\,\mathrm{m/s}$, showing that the product $B^2 L_U$ is too low for such a model boat. Considering the pump part, we

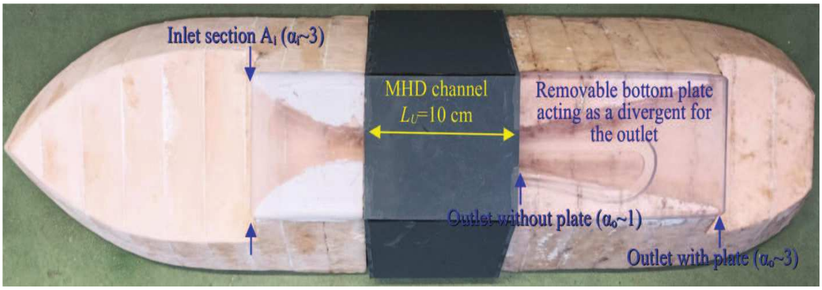

Fig. 8. Model boat, bottom view.

have $U_a = 3.7 \times 10^3$, $I_a = 1.2 \times 10^7$, $\Delta p_{\mathrm{ta}} = 6.8 \times 10^6$ (see Eq. (15)), and $\eta_{\mathrm{pump}} = 0.016\%$, i.e. parameters far out of the interesting zone plotted in Fig. 2.

Upscaling is favourable, but insufficient since U_a is only proportional to L^{-1}. A boat with $L_U = 10\,\mathrm{m}$, if B, α_{SCD} and k_{tot} are unchanged, would reach $V_\infty = 0.3\,\mathrm{m/s}$ at $I_a = 1240$ and $U_a = 37$, which is still too high to have a reasonable pump (and boat) efficiency. Increasing B is also needed, i.e. we have to use superconducting magnets. For example, with $B = 10\,\mathrm{T}$, $L_U = 5\,\mathrm{m}$, α_{SCD} and k_{tot} unchanged, we have $V_{\mathrm{ref}} = 1.4\,\mathrm{m/s}$ and we can reach $V_\infty = 3\,\mathrm{m/s}$ with a boat efficiency $\eta = 8.8\%$ (and $\eta_{\mathrm{pump}} = 17\%$). Furthermore, the loss and drag coefficient decrease for large scales (our model boat is penalized by a very strong relative rugosity of its channel). Dividing those coefficients by two, i.e. for $B = 10\,\mathrm{T}$, $L_U = 5\,\mathrm{m}$, $k_{\mathrm{tot}} = 0.5$ and $\alpha_{\mathrm{SCD}} = 2.45$, we reach $V_\infty = 3\,\mathrm{m/s}$ for $I_a = 2.13$, with a thruster efficiency $\eta = 20\%$ (and $\eta_{\mathrm{pump}} = 31\%$ if $k_{\mathrm{loss}} = 0.4$). With that superconducting thruster, the drag and internal losses reduced ($C_{\mathrm{D}} = 0.135$, $k_{\mathrm{tot}} = 0.5$), the boat scaled up by a factor 50 needs $P_{\mathrm{channel}} = 400\,\mathrm{kW}$ to reach $V_\infty = 3\,\mathrm{m/s}$.

Conclusion.

Starting from a pump experiment and its CFD detailed description, a simple model is proposed here, where the MHD channel is characterized by a loss coefficient, and the running point of the pump by two other dimensionless parameters (I_a, U_a). Such a pump (equipped with permanent magnets) was installed in a small experimental model boat described by two additional dimensionless parameters (additional losses and α_{SCD}). The resulting model can be used for upscaling, with quick turnaround time, in the pre-design phase of MHD pumps and thrusters.

Acknowledgements. We thank LEGI's support teams, who built the pump and propeller, and the students who worked on the boat during their projects or internships.

References

[1] Y. Sasakawa (ed.). *Yamato-1, world first superconducting MHD propulsion ship.* Ship and Ocean foundation (1997).

[2] C. Senatore, M. Bonura, T. Bagni. REBCO tapes for applications in ultra-high fields: critical current surface and scaling relations. *Supercond. Sci. Technol*, vol. 37 (2024), p. 115013.

[3] E. Martin-Lopez, Y. Delannoy, F. Benoit, R. Martinie, S. Vitry. Numerical and experimental validation of the performance of an electromagnetic pump for a sodium fast reactor. In: *Proc. ICAPP'17* (Fukui and Kyoto, Japan, April 24–28, 2017).

[4] Y. Delannoy, V. Roche. Elamhyd, électrochimie des actionneurs magnétohydrodynamiques en eau de mer. *Carnot Energies Day* (Grenoble, 2021).

[5] I.E. Idelchik. *Handbook of Hydraulic Resistance* (New York: Begell House 2021).

[6] B. Zhao *et al.* Experimental study on superconducting helical channel MHD thruster. In: *Proc. The 42nd AIAA Plasmadynamics and Lasers Conference* (Honolulu, Hawaii, 2011).

[7] H. Zhang *et al.* Comparison of computational fluid dynamic simulation of a stirred tank with polyhedral and tetrahedral meshes. *Iran. J. Chem. Chem. Eng.*, vol. 39 (2020), pp. 311–319.

Received 24.11.2024